Non-Oscillatory Boundary Treatment
for Staggered Central Schemes

Doron Levy[†]   Eitan Tadmor[‡]

August 16, 1998

Abstract

We are concerned with high-resolution, non-oscillatory *central* schemes for approximating solutions of nonlinear, multi-dimensional, hyperbolic conservation laws subject to prescribed initial values and to Dirichlet boundary conditions in inflow boundaries. We demonstrate that a naive continuation of these central schemes up to the boundary typically results in spurious oscillations at inflow boundaries. Consequently, we are led to present our new boundary scheme which is based on a different treatment in inflow and in outflow boundaries. We explicitly construct the boundary scheme in one and in two space dimensions and present numerical simulations that clearly demonstrate its desired non-oscillatory properties.

Contents

1 Introduction

In recent years, central schemes for approximating solutions of hyperbolic conservation laws, received a lot of attention. In particular, a family of high-resolution, non-oscillatory, *central* schemes, was developed to handle such problems. Compared with the 'classical' *upwind* schemes, these *central* schemes were shown to be both simple and stable for a large variety of problems ranging from one-dimensional scalar problems to multi-dimensional systems of

---

[†]Département de Mathématiques et d'Informatique, Ecole Normale Supérieure, 45 rue d'Ulm, 75230 Paris Cedex 05, France; dlevy@dmi.ens.fr

[‡]School of Mathematical Sciences, Tel-Aviv University, Tel-Aviv 69978, Israel; and Department of Mathematics, UCLA, Los-Angeles CA 90095; Email: tadmor@math.ucla.edu

conservation laws. They were successfully implemented for a variety of other related problems, such as, e.g., the incompressible Euler equations [18], the magneto-hydrodynamics equations [28], hyperbolic systems with relaxation source terms [3], non-linear optics [23] and slow moving shocks [11].

The high-order *central* schemes can be viewed as a direct extension to the first-order, Lax-Friedrichs (LxF) scheme [6], which on one hand is robust and stable, but on the other hand suffers from excessive dissipation. To address this problematic property of the LxF scheme, a Godunov-like second-order central scheme was developed by Nessyahu and Tadmor (NT) in [20] (see also [25]). It was extended to higher-order of accuracy as well as for more space dimensions (consult [1, 2, 10, 12, 15, 17] for the two-dimensional case, and [24, 19, 4, 16] for higher-order methods).

The NT scheme is based on reconstructing, in each time step, a piecewise-polynomial interpolant from the cell-averages computed in the previous time step. This interpolant is then (exactly) evolved in time, and finally projected on its staggered averages, resulting with the staggered cell-averages at the next time-step. The one- and two-dimensional second-order schemes, are based on a piecewise-linear MUSCL-type reconstruction, whereas the higher-order schemes are based on piecewise-polynomial reconstructions of higher-order.

Like *upwind* schemes, the reconstructed piecewise-polynomials used by the central schemes, also make use of non-linear limiters which guarantee the overall non-oscillatory nature of the approximate solution. Yet, unlike the upwind schemes, central schemes avoid the intricate and time consuming Riemann solvers; this advantage is particularly important in the multi-dimensional setup – where no such Riemann solvers exist.

In this paper, we address the question of implementing the central schemes in the presence of *Dirichlet boundary conditions in inflow boundaries*. First, we demonstrate that a naive continuation of the central scheme from the interior of the domain up to the boundary may result in spurious oscillations. Consequently, we are led to introduce a new accurate boundary scheme which is problem independent and also enjoys the overall simplicity and advantages of the central framework.

The paper is organized as follows:

In §2 we briefly overview the construction of the central schemes, focusing on the one- and two-dimensional second-order scheme.

In §3 we turn to deal with the problem of augmenting the central methods with Dirichlet boundary conditions prescribed in inflow boundaries. After showing that a naive approach of extending the interior treatment to the boundary can produce spurious oscillations, we present our new boundary method. This method is based on a separate treatment of the *inflow* and *outflow* boundaries. In both cases we still construct a linear interpolant in the boundary cells. While in outflow boundary cells, a one-sided reconstruction based on data propagating from the interior of the domain is natural, in the inflow case, however, one has to take into account also the point-wise data from the boundary. The key question which we answer here is exactly how to plug this inflow data into the approximate solution without modifying the accuracy of the method, and without creating numerical artifacts.

We end in §4 by presenting several examples in which our new boundary method is implemented. These examples clearly show that our treatment does not produce any spurious oscillations at the boundary while retaining the overall order of accuracy, and by that it clearly enjoys the robust nature of the entire interior schemes.

2 A Short Guide to Central Schemes

In this section we briefly overview the construction of high-order, non-oscillatory, central schemes for approximating solutions of hyperbolic conservation laws. We start by considering the one-dimensional hyperbolic system of conservation laws

$$u_t + f(u)_x = 0, \tag{2.1}$$

subject to the initial data, $u(x, t{=}0) = u_0(x)$. To approximate solutions of (2.1), we introduce a mesh in the $x - t$ plane, the spatial grid-points are denoted by x_j. We denote by Δx and Δt, the spacing in the x and in the t variables respectively, and abbreviate by I_j the cell around x_j, i.e., $I_j := \left\{ \xi \mid \|\xi - x_j\| \leq \frac{\Delta x}{2} \right\}$.

By $w_j \sim u(x_j)$, we denote the approximate solution at x_j, and define $\bar{w}_j$ as the average of w_j over the cell I_j. Here, we follow Nessyahu and Tadmor (NT) [20] in the reconstruction of the second-order, non-oscillatory central scheme. To approximate solutions of (2.1), we introduce a piecewise-linear approximate solution at the discrete time levels, $t^n = n\Delta t$, based on linear functions $p_j(x, t^n)$ which are supported at the cells I_j,

$$w(x, t)|_{t=t^n} = \sum_j p_j(x, t^n)\chi_j(x) := \sum_j \left[\bar{w}_j^n + w_j' \left(\frac{x - x_j}{\Delta x} \right) \right] \chi_j(x), \quad \chi_j(x) := 1_{I_j}. \tag{2.2}$$

Second-order of accuracy is guaranteed if the discrete slopes approximate the corresponding derivatives, $w_j' \sim \Delta x \cdot \partial_x w(x_j, t^n) + O(\Delta x)^2$. Such a non-oscillatory approximation of the derivatives is possible, e.g., by using built-in non-linear limiters of the form

$$w_j' = MM\{\theta(\bar{w}_{j+1}^n - \bar{w}_j^n), \frac{1}{2}(\bar{w}_{j+1}^n - \bar{w}_{j-1}^n), \theta(\bar{w}_j^n - \bar{w}_{j-1}^n)\}. \tag{2.3}$$

Here and below, $\theta \in (0, 2)$ is a non-oscillatory limiter and MM denotes the Min-Mod function

$$MM\{x_1, x_2, ...\} = \begin{cases} \min_i\{x_i\} & \text{if } x_i > 0, \forall i \\ \max_i\{x_i\} & \text{if } x_i < 0, \forall i \\ 0 & \text{otherwise.} \end{cases}$$

An *exact* evolution of w, based on integration of the conservation law over the staggered cell, $I_{j+\frac{1}{2}}$, then reads

$$\bar{w}_{j+\frac{1}{2}}^{n+1} = \frac{1}{\Delta x} \int_{I_{j+\frac{1}{2}}} w(x, t^n)dx - \frac{1}{\Delta x} \int_{\tau=t^n}^{t^{n+1}} \left[f(w(x_{j+1}, \tau)) - f(w(x_j, \tau)) \right] d\tau.$$

The first integral is the staggered cell-average at time t^n, $\bar{w}_{j+\frac{1}{2}}^n$, which can be computed directly from the above reconstruction. The time integrals of the flux are computed by the second-order accurate mid-point quadrature rule. Here, the Taylor expansion is being used to predict the required mid-values of w. The scheme can be therefore formulated in a predictor-corrector form: a *predictor step*

$$w_j^{n+1/2} = w_j^n - \frac{\lambda}{2}f_j', \qquad f_j' = f_u(w_j)w_j' =: A(w_j)w_j', \tag{2.4}$$

which is followed by the *corrector* step

$$\bar{w}_{j+\frac{1}{2}}^{n+1} = \frac{1}{2}(\bar{w}_j^n + \bar{w}_{j+1}^n) + \frac{1}{8}(w_j' - w_{j+1}') - \lambda \left[f(w_{j+1}^{n+1/2}) - f(w_j^{n+1/2}) \right]. \tag{2.5}$$

To upgrade this scheme into a third-order accurate scheme, e.g., one has to use (consult [19])

- A piecewise-parabolic reconstruction which replaces the piecewise-linear reconstruction.

- A more accurate quadrature rule for the flux integral such as Simpsons method, which replaces the mid-point quadrature.

- A second-order accurate Taylor expansion to predict the mid-values which replaces the corresponding first-order expansion. Alternatively, one can replace the Taylor expansion with a Runge-Kutta solver (consult [4], [16]), which is a favorable approach in particular for systems.

Following the same ideas, one can derive a non-oscillatory, two-dimensional central scheme. Below we sketch the construction of the second-order two-dimensional scheme following [10]. For a two-dimensional third-order accurate scheme, we refer to [15], [17].

We consider the two-dimensional hyperbolic system of conservation laws

$$u_t + f(u)_x + g(u)_y = 0. \tag{2.6}$$

To approximate a solution to (2.6), we start with a two-dimensional linear reconstruction

$$w(x, y, t^n) = \sum_{j,k} p_{j,k}(x, y) \chi_{j,k}(x, y), \tag{2.7}$$

$$p_{j,k}(x, y) = \bar{w}_{j,k}^n + w_{j,k}' \left(\frac{x - x_j}{\Delta x} \right) + w_{j,k}^{\backslash} \left(\frac{y - y_k}{\Delta y} \right).$$

Here, the discrete slopes in the x and in the y direction approximate the corresponding derivatives, $w_{j,k}' \sim \Delta x \cdot w_x(x_j, y_k, t^n) + O(\Delta x)^2$, $w_{j,k}^{\backslash} \sim \Delta y \cdot w_y(x_j, y_k, t^n) + O(\Delta y)^2$, and $\chi_{j,k}(x, y)$ is the characteristic function of the cell $I_{j,k} := \left\{ (\xi, \eta) | |\xi - x_j| \leq \frac{\Delta x}{2}, |\eta - y_k| \leq \frac{\Delta y}{2} \right\}$.

An exact evolution of this reconstruction, which is based on integration of the conservation law over the staggered volume followed by a mid-point approximation to the integrals of the fluxes, can be formulated in a predictor-corrector form with the *predictor step*

$$w_{j,k}^{n+\frac{1}{2}} = w_{j,k}^n - \frac{\lambda}{2} f_{j,k}' - \frac{\mu}{2} g_{j,k}^{\backslash}, \tag{2.8}$$

and the *corrector step*

$$\begin{aligned}
\bar{w}_{j+\frac{1}{2},k+\frac{1}{2}}^{n+1} &= \; < \frac{1}{4}(\bar{w}_{j,\cdot}^n + \bar{w}_{j+1,\cdot}^n) + \frac{1}{8}(w_{j,\cdot}' - w_{j+1,\cdot}') - \lambda(f_{j+1,\cdot}^{n+\frac{1}{2}} - f_{j,\cdot}^{n+\frac{1}{2}}) >_{k+\frac{1}{2}} + \\
&+ \; < \frac{1}{4}(\bar{w}_{\cdot,k}^n + \bar{w}_{\cdot,k+1}^n) + \frac{1}{8}(w_{\cdot,k}^{\backslash} - w_{\cdot,k+1}^{\backslash}) - \mu(g_{\cdot,k+1}^{n+\frac{1}{2}} - g_{\cdot,k}^{n+\frac{1}{2}}) >_{j+\frac{1}{2}}.
\end{aligned}$$

Here are below, $\lambda := \frac{\Delta t}{\Delta x}$ and $\mu := \frac{\Delta t}{\Delta y}$ denote the fixed mesh-ratios, and we used the staggered averaging notation

$$< w_{j,\cdot} >_{k+\frac{1}{2}} := \frac{1}{2}(w_{j,k} + w_{j,k+1}), \qquad < w_{\cdot,k} >_{j+\frac{1}{2}} := \frac{1}{2}(w_{j,k} + w_{j+1,k}).$$

3   Numerical Treatment of Boundary Conditions

In this section we construct a non-oscillatory boundary scheme that augments the second-order interior central scheme we overviewed in §2. We start by constructing such a scheme for the one-dimensional case and then extend this boundary scheme to two space dimensions.

3.1   The scalar One-Dimensional Setup

The *central* schemes we overviewed in §2 are based on a staggered grid. Consequently, the boundary scheme we present here is composed from two steps dictated by the two phases of the boundary cells. While one stencil is composed of whole cells, the staggered stencil terminates with half-cells at both boundaries (see Figure 1).
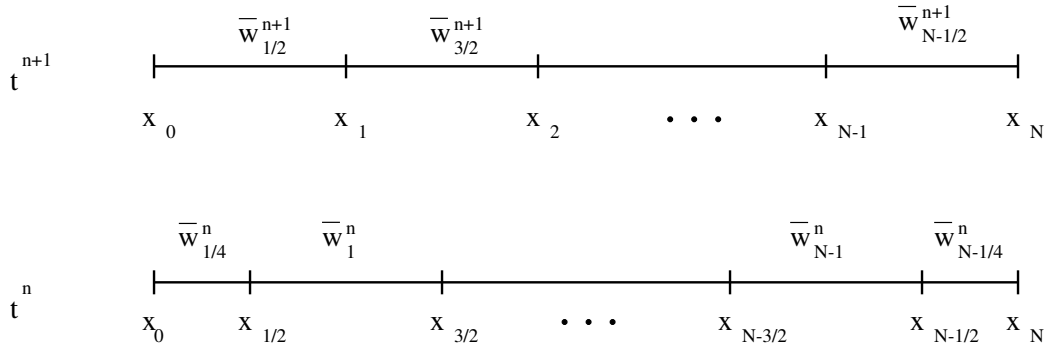

Figure 1: one dimensional stencil

The Problem

We start by demonstrating that a naive continuation of the interior central scheme up to the boundary, typically results with spurious oscillations. To this extent, we assume that the cell-averages, $\bar{w}_{1/2}^n, \bar{w}_{3/2}^n \ldots, \bar{w}_{N-1/2}^n$, are known and we wish to compute $\bar{w}_{1/4}^{n+1}$, $\bar{w}_j^{n+1}$ $(j=1,\ldots,N-1)$, $\bar{w}_{N-\frac{1}{4}}^{n+1}$ at the next time-step (a reversed situation compared with Figure 1). We assume that the left boundary is an *inflow* boundary and hence data propagates into the interior of the domain. Consequently, the point-values at the boundary, w_0, must be prescribed.

At such an inflow boundary-cell, $I_{1/2}$, the reconstructed interpolant is given by (consult (2.2))

$$p_{1/2}(x, t^n) = \bar{w}_{1/2}^n + w_{1/2}' \left(\frac{x - x_{1/2}}{\Delta x} \right). \tag{3.1}$$

The cell-average, $\bar{w}_{1/2}^n$, was already computed at the previous time-step; the remaining question is how to reconstruct the discrete slope, $w_{1/2}'$, at the boundary cell, $I_{1/2}$? Here we are dealing with an inflow boundary and thus the point-value, w_0^n, is prescribed. Consequently, we may use the prescribed boundary point-values to uniquely determine the discrete slope, $w_{1/2}'$, as

$$w_{1/2}' = 2(\bar{w}_{1/2}^n - w_0^n). \tag{3.2}$$

Here, due to the unique solution (3.2), one can not limit the discrete slope at the boundary cell by using the limiting procedure which was used to prevent spurious oscillations at the interior

cells (see (2.3)). Consequently, the reconstruction (3.1) can develop spurious oscillations at the boundary, which will then propagate and contaminate also the interior of the domain.

In Figure 2 we demonstrate a typical situations in which spurious oscillations develop at the boundary. Here, we solve Burgers equation: (2.1) with $f(u) = u^2/2$, augmented with the initial data

$$u_0(x) = -5x^3, \quad x \in [-1, 1],$$

and with the inflow boundary conditions, $u(-1, t) = 5$, $u(1, t) = -5$. On the boundary cells, we use a linear reconstruction whose slopes where determined according to (3.2).
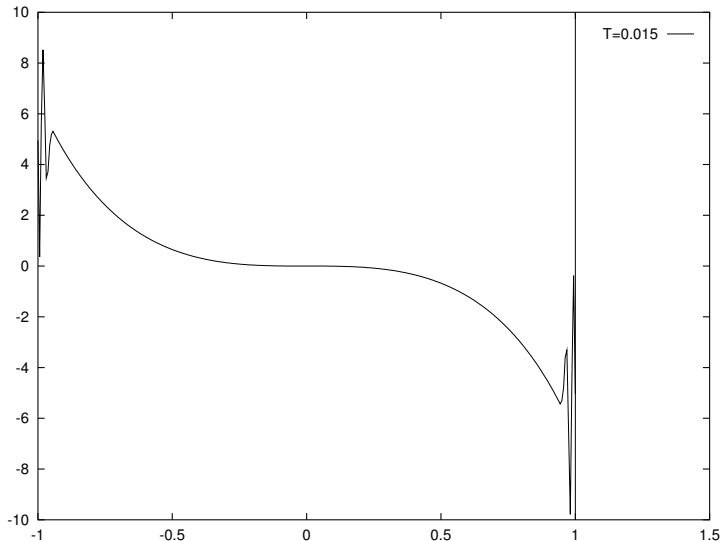

Figure 2: Oscillations at the boundaries with naive boundary treatment

The Solution

In the following we present our new boundary scheme at the left boundary. An analogous treatment holds for the right boundary. First, we assume that the cell averages, $\bar{w}^n_{1/4}$, $\bar{w}^n_{j\,(j=1,\ldots,N-1)}$, $\bar{w}^n_{N-\frac{1}{4}}$, are given at time $t = t^n$, and we wish to compute the cell averages, $\bar{w}^{n+1}_{1/2}, \bar{w}^{n+1}_{3/2} \ldots, \bar{w}^{n+1}_{N-1/2}$, at the next time-step t^{n+1} (consult Figure 1).

To follow the setup dictated by the differential level, we distinguish between two possible situations: the left boundary is either an *inflow* boundary, i.e., $f'(\bar{w}^n_{1/4}) > 0$, or an *outflow* boundary, $f'(\bar{w}^n_{1/4}) < 0$.

If it is an *inflow* boundary cell, we replace the given cell-average, $\bar{w}^n_{1/4}$, with the prescribed boundary data at the left of the cell, w^n_0, i.e., we define

$$\bar{w}^n_{1/4} := w^n_0.$$

Such an assignment enables us to construct a linear interpolant that coincides with the boundary data on x_0. This is equivalent to considering instead of the half cell, a whole cell $I_0 = [x_{-1/2}, x_{1/2}]$, centered around x_0. We note that the computation of the derivative in the neighboring cell I_1, therefore involves the cell-averages, $\bar{w}^n_1, \bar{w}^n_2$, and the prescribed point-value, w^n_0.

The reconstructed linear interpolant at the boundary cell I_0 equals

$$p_0(x, t^n) = \bar{w}_{1/4}^n + w_{1/4}' \left(\frac{x - x_0}{\Delta x} \right), \qquad x \in [x_0, x_{1/2}].$$

The required derivative, $w_{1/4}'$, is approximated using a one sided derivative, i.e., $w_{1/4}' = \bar{w}_1^n - w_0^n$. It is easy to see that this one-sided computation of the derivative avoids over/under-shoots and hence it is free from spurious oscillations. The point-values on the boundary at the mid-time, $w_0^{n+1/2}$, required for the approximation of the flux integral there, is assumed to be given (from the inflow data). In fact, assuming that the data at an inflow boundary is prescribed for all time, one can approximate the flux integral there as accurate as desired.

In the *outflow* case, the only change compared with the inflow case is that there is no given boundary data. The approximation of the derivative is once again one-sided, $w_{1/4}' = \bar{w}_1^n - w_0^n$, and the required mid-value on the boundary itself is computed using the standard Taylor predictor step.

In the second phase of the staggering, we assume that the cell-averages, $\bar{w}_{1/2}^{n+1}, \bar{w}_{3/2}^{n+1}, \ldots$, are given, and we compute the cell averages at the next time step, $\bar{w}_{1/4}^{n+2}, \bar{w}_j^{n+2} (j=1,\ldots,N), \bar{w}_{N-1/4}^{n+2}$.

Here, the crucial observation is that in order to avoid spurious oscillations, one must use one-sided approximations of the derivatives from the interior of the domain in the boundary cells in both inflow and outflow cases. Locally, in inflow boundary cells in this phase of the staggering, one can not satisfy the non-oscillatory requirements and simultaneously agree with the given boundary conditions as demonstrated above. The key point is that ignoring the exact point-values at the boundary in one phase is allowed, as the exact values are plugged into the approximate solution in the next time step. Alternatively, one can interpret this step as an intermediate step in which one splits the cell $I_{1/2}$ into two: $I_{1/2} = [x_0, x_0+\epsilon] \cup [x_0+\epsilon, x_1]$, where $\epsilon \sim (\Delta x)^2$. In the right part, $[x_0 + \epsilon, x_1]$, one implements a one-sided approximation of the derivative, while the left part, $[x_0, x_0+\epsilon]$, is non-important as its contribution is overridden in the next phase of the staggering when we exchange the computed cell-average with the given point-value at an inflow boundary cell.

Following this idea, one uses one-sided approximation for the derivative, $w_{1/2}' = \bar{w}_{3/2}^{n+1} - \bar{w}_{1/2}^{n+1}$. The slope in any piecewise-linear cell is constant throughout the cell, and in particular, $w_0' = w_{1/2}'$. Utilizing a Taylor expansion, the predicted mid-value at the boundary equals

$$w_0^{n+3/2} = w_0^{n+1} - \frac{\lambda}{2} f_0', \tag{3.3}$$

with

$$w_0^{n+1} = w_{1/2}^{n+1} - \frac{\Delta x}{2} w_{1/2}', \qquad f_0' = A(w_0^{n+1}) w_0', \qquad w_0' = w_{1/2}'.$$

The boundary cell average at t^{n+2} is given by integration over the control volume $I_{1/4} \times [t^{n+1}, t^{n+2}]$, which leads to the *corrector step*

$$\bar{w}_{1/4}^{n+2} = \bar{w}_{1/2}^{n+1} - \frac{1}{4} w_{1/2}' - \lambda \left[f(w_{1/2}^{n+3/2}) - f(w_0^{n+3/2}) \right]. \tag{3.4}$$

Remark: We emphasize that the exact point-values prescribed by the Dirichlet boundary condition at inflow boundaries enter only in one phase of the staggering. The one-sided extrapolation of the approximated derivatives on the boundary cells is the same for both inflow and

outflow cases. One may think of overcoming the difficulty in understanding why the boundary conditions enter only in one phase of the staggering, by looking at the entire method every two time steps. The surprising point, however, is that in view of the above, it is natural to consider the basic stencil of such two-step method, as the one composed of the half-cells at the boundaries, because this is the stencil in which the inflow data enters.

The entire boundary scheme is summarized in the following algorithm:

Phase I (of the staggering):
  Determine the type of the flow at the left boundary. If inflow ($f'(w_{1/4}^n) > 0$):

  $\bar{w}_{1/4}^n := w_0^n$ Exchanging the cell-average for the boundary data.

  $w_0^{n+1/2}$ Given by the boundary data.
  In both inflow and outflow cases:

  $w_0' = \bar{w}_1^n - \bar{w}_{1/4}^n$ One sided approximation of the derivative.

Phase II:

  $w_{1/2}' = \bar{w}_{3/2}^{n+1} - \bar{w}_{1/2}^{n+1}$ One-sided approximation.

  $w_0^{n+1} = w_{1/2}^{n+1} - \frac{\Delta x}{2} w_{1/2}', \quad f_0' = A(w_0^{n+1}) w_{1/2}'$

  $w_0^{n+3/2} = w_0^{n+1} - \frac{\lambda}{2} f_0'$

  $\bar{w}_{1/4}^{n+2} = \bar{w}_{1/2}^{n+1} - \frac{1}{4} w_{1/2}' - \lambda[f(w_{1/2}^{n+3/2}) - f(w_0^{n+3/2})]$ The half cell-average at the boundary.

In the case of an inflow boundary, replace $w_0^{n+3/2}$ with the exact value.

3.2 Extensions to Systems

An analogous boundary treatment to the scalar case presented in §3.1 is also valid for systems. The distinction between inflow and outflow boundaries is crucial for the well-posedness of the underlying problem. Technically, however, assuming that the consistency of the problem is given, there is almost no difference between our handling of the two types of boundaries. One simply introduces the given data when such is available, either as cell-averages or as point-values (for the quadrature of the fluxes)

As shown in §3.1 above, it is forbidden to utilize the point-values at the inflow boundaries for limiting the derivatives there, as this may introduce spurious oscillations as demonstrated above. Derivatives on the boundary should be computed using one-sided approximations.

Following these ideas, the extension to systems is straightforward. Systems are solved component-wise (consult [20]). Each component is treated at the boundary exactly like the scalar case of §3.1.

3.3 Extensions to the Two-Dimensional Setup

Here, we extend the one-dimensional boundary scheme presented in §3.1, to the two-dimensional setup. This extension is done dimension by dimension; in each direction we apply the one-dimensional arguments. Following §3.1, in the phase of the staggering that involved half-cells, we replace the cell-averages with the given boundary conditions in inflow cells. All derivatives in the boundary cells, at both phases of the staggering, are computed using one-sided approximations. Finally, the required mid-values on the boundary are either extrapolated from the interior in outflow cells, or taken from the given data in inflow cells.

For brevity, we only consider the left boundary and the upper-left corner. An analogous treatment holds for the other three boundaries and corners. We recall that in this two-dimensional case, we approximate solutions to equation (2.6), augmented with boundary conditions at the inflow boundaries.
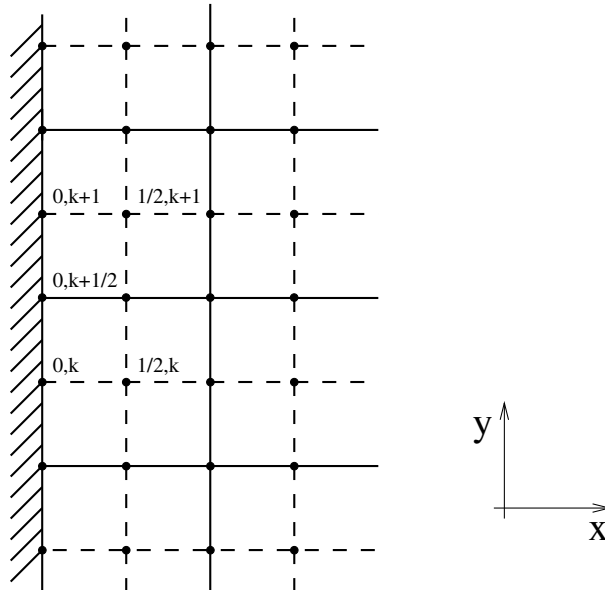

Figure 3: Two dimensions - left boundary

We start with the first phase of the staggering assuming that the cell-averages are given on the stencil which is composed of partial-cells at the boundary (the dotted stencil in Figure 3). We consider the left boundary, and distinguish between *inflow* $(f'(w^n_{1/4,k+1/2}) > 0)$, and *outflow* $(f'(w^n_{1/4,k+1/2}) < 0)$, boundary cells. Following the one-dimensional arguments, in inflow cells, we replace the cell-average with the boundary data, i.e.,

$$\bar{w}^n_{1/4,k+1/2} := w^n_{0,k+1/2}.$$

The x-derivative is computed in both inflow and outflow boundaries using a one-sided approximation,

$$w'_{1/4,k+1/2} = \bar{w}^n_{1,k+1/2} - \bar{w}^n_{1/4,k+1/2}.$$

The y-derivative is computed using the same limiting mechanism of the interior scheme. The rest of the computations is straightforward, noting that in inflow boundary cells, the mid-values, $w^{n+1/2}_{0,k+1/2}$, are known from the boundary condition.

We now turn to the corners and as a prototype, consider the upper-left corner (see Figure 4). In the corner we repeat the previous boundary treatment with one simple modification, namely, we replace the cell average with the boundary data whenever *at least* one of the two directions (x or y) is an *inflow* boundary,

$$\bar{w}^n_{1/4,N-1/4} := w_{0,N}.$$

Both derivatives are computed using one-sided approximations,

$$
\begin{aligned}
w'_{1/4,N-1/4} &= \bar{w}^n_{1,N-1/4} - \bar{w}^n_{1/4,N-1/4}, \\
w^{\backslash}_{1/4,N-1/4} &= \bar{w}^n_{1/4,N-1/4} - \bar{w}^n_{1/4,N-1}.
\end{aligned}
$$

The mid-value at the corner, $w_{0,N}^{n+1/2}$, is either taken from the boundary data if at least on of the boundaries is inflow, or approximated using a Taylor expansion if its an outflow corner in both directions.
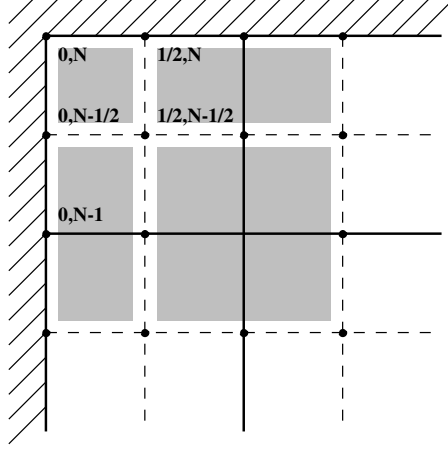

Figure 4: Upper-left corner

We now turn to the second phase of the staggering. For simplicity of notation, we assume that the cell-averages are given in time t^n, and we would like to compute the staggered cell-averages at time t^{n+1}.

We start with the left boundary (consult Figure 3). First, the discrete slope in the x-direction are computed using the one-sided approximation $w'_{1/2,k} = \bar{w}^n_{3/2,k} - \bar{w}^n_{1/2,k}$. In the inflow case, the mid-values $w_{0,k}^{n+1/2}$ are prescribed by the boundary conditions. In the outflow case, we extrapolate these values from the interior, i.e., first we have

$$w_{0,k}^n = w_{1/2,k}^n - \frac{\Delta x}{2} w'_{1/2,k},$$

which is then used to predict the mid-value,

$$w_{0,k}^{n+1/2} = w_{0,k}^n - \frac{\lambda}{2} f'_{0,k} - \frac{\mu}{2} g^\backslash_{0,k}.$$

Here $f'_{0,k} = A(w_{0,k}^n) w'_{1/2,k}$ and $g^\backslash_{0,k} = B(w_{0,k}^n) w^\backslash_{1/2,k}$. The discrete slope in the y-direction, $w^\backslash_{0,k}$, is computed in both inflow and outflow cases using the limiting procedure of the interior scheme. Finally, the staggered average at time t^{n+1} is given by

$$
\begin{aligned}
\bar{w}_{1/4,k+1/2}^{n+1} \;=\; & \frac{\bar{w}^n_{1/2,k} + \bar{w}^n_{1/2,k+1}}{2} + \frac{1}{8}(-w'_{1/2,k} - w'_{1/2,k+1} + w^\backslash_{1/2,k} - w^\backslash_{1/2,k+1}) - \\
& - \frac{\lambda}{2}(f(w^n_{1/2,k+1}) + f(w^n_{1/2,k}) - f(w^n_{0,k+1}) - f(w^n_{0,k})) - \\
& - \mu(g(w^n_{1/2,k+1}) + g(w^n_{0,k+1}) - g(w^n_{1/2,k}) - g(w^n_{0,k+1})).
\end{aligned}
\tag{3.5}
$$

This concludes the boundary treatment of the left boundary. Similar expressions hold for the other three boundaries.

We are left with the corners. Once again, we consider the upper-left corner (see Figure 4). If the flow in this corner is outflow in both directions, the required quantities for the computation

of the cell-averages at the next time-step are computed according to

$$
\begin{cases}
w'_{1/2,N-1/2} = \bar{w}^n_{3/2,N-1} - \bar{w}^n_{1/2,N-1/2}, & \text{One-sided slopes} \\[2mm]
w^{\backslash}_{1/2,N-1/2} = \bar{w}^n_{1/2,N-1/2} - \bar{w}^n_{1/2,N-3/2},
\end{cases}
$$

$$
\begin{cases}
w^n_{0,N-1/2} = w^n_{1/2,N-1/2} - \frac{\Delta x}{2} w'_{1/2,N-1/2}, & \text{Predictor (west)} \\[2mm]
w^{n+1/2}_{0,N-1/2} = w^n_{0,N-1/2} - \frac{\lambda}{2} f'_{0,N-1/2} - \frac{\mu}{2} g^{\backslash}_{0,N-1/2},
\end{cases}
$$

$$
\begin{cases}
w^n_{1/2,N} = w^n_{1/2,N-1/2} + \frac{\Delta y}{2} w^{\backslash}_{1/2,N-1/2}, & \text{Predictor (north)} \\[2mm]
w^{n+1/2}_{1/2,N} = w^n_{1/2,N} - \frac{\lambda}{2} f'_{1/2,N} - \frac{\mu}{2} g^{\backslash}_{1/2,N},
\end{cases}
$$

$$
\begin{cases}
w^n_{0,N} = w^n_{1/2,N-1/2} - \frac{\Delta x}{2} w'_{1/2,N-1/2} + \frac{\Delta y}{2} w^{\backslash}_{1/2,N-1/2}, & \text{Predictor (north-west)} \\[2mm]
w^{n+1/2}_{0,N} = w^n_{0,N} - \frac{\lambda}{2} f'_{0,N} - \frac{\mu}{2} g^{\backslash}_{0,N}.
\end{cases}
$$

In an inflow boundary, the predicted mid-values are replaced by the boundary data, i.e., either $\{w^{n+1/2}_{0,N-1/2}, w^{n+1/2}_{0,N}\}$ or $\{w^{n+1/2}_{1/2,N}, w^{n+1/2}_{0,N}\}$ or all three if it is an inflow-inflow corner.

The cell-average in the north-west edge of Figure 4 in time t^{n+1}, is finally given by the *corrector step*

$$
\begin{aligned}
\bar{w}^{n+1}_{1/4,N-1/4} = {} & \bar{w}^n_{1/2,N-1/2} + \frac{-w'_{1/2,N-1/2} + w^{\backslash}_{1/2,N-1/2}}{4} - \\
& -\lambda(f(w^n_{1/2,N}) + f(w^n_{1/2,N-1/2}) - f(w^n_{0,N}) - f(w^n_{0,N-1/2})) - \\
& -\mu(g(w^n_{1/2,N}) + g(w^n_{0,N}) - g(w^n_{1/2,N-1/2}) - g(w_{0,N-1/2})^n).
\end{aligned}
\tag{3.6}
$$

4 Examples of Non-Linear Initial-Boundary Value Problems

Accuracy tests

We start by presenting a couple of accuracy tests. The first accuracy test, taken from [26], corresponds to the linear advection problem $u_t + u_x = 0$ in the domain [-1,1], subject to the time-dependent boundary condition $u(-1,t) = \sin \pi t$ and to the initial data $u(x,0) = \sin \pi x$. In Table 1 we present the L_1 and L_∞ errors and convergence rates obtained at time $T = 1$ with $CFL = 0.49$. As expected, our boundary scheme preserves the order of accuracy of the method, and results with a second-order method when measured in the L_1 norm.

In Table 2 we present the results obtained when computing the accuracy of our method with the Burgers equation, $u_t + u u_x = 0$ in the domain [-1,1]. Here, the initial data was taken as $u_0(x) = 2 + \cos[\pi(x + 0.25)]$, and the time-dependent data in the left inflow boundary was taken as the exact solution of the periodic Burgers equation at $x = -1$, with the same initial data. Once again, it is evident that our method is second-order.

N	L_1 error	L_1 order	L_∞ error	L_∞ order
40	1.363e-3	-	3.611e-3	-
80	3.484e-4	1.97	1.328e-3	1.44
160	8.805e-5	1.98	6.205e-4	1.10
320	2.288e-5	1.94	2.819e-4	1.14
640	5.861e-6	1.96	1.161e-4	1.28

Table 1: Linear Advection, $T = 1$, $CFL = 0.49$. L_1 and L_∞ errors and convergence rates.

N	L_1 error	L_1 order	L_∞ error	L_∞ order
40	7.169e-3	-	2.176e-2	-
80	1.952e-3	1.88	8.986e-2	1.28
160	5.284e-4	1.89	3.650e-3	1.30
320	1.444e-4	1.87	1.519e-3	1.26
640	3.798e-5	1.93	6.172e-4	1.30

Table 2: Burgers Equation, $T = 0.15$, $CFL = 0.49$. L_1 and L_∞ errors and convergence rates.

Shock exiting the domain

Our next example is of a shock going out of the domain. Here, we approximate the solution of the one-dimensional Burgers Equation,

$$u_t + \left(\frac{u^2}{2}\right)_x = 0, \qquad -1 \le x \le 1, \quad 0 \le t, \tag{4.1}$$

subject to the initial conditions, $u_0(x) = 0.2 - \sin\left(\frac{\pi x}{2}\right)$, and to the constant inflow boundary conditions, $u(-1) = u_0(-1) = 1.2$, $u(1) = u_0(1) = -0.8$. In time, the solution sharpens until a discontinuity (shock) is formed. This shock moves towards the right boundary and disappears after 'hitting' it.

Figure 5 shows the evolution of the numerical solution to equation (4.1) in time. The plotted values are the cell-averages. One can clearly see the formation of the shock, and its movement towards the right boundary. Note that no spurious oscillations are created in the boundaries.

Shock entering from inflow-boundary

Our last 1D example is that of a shock entering the domain from a time-dependent inflow boundary. Following Cockburn and Shu [5], we solve the Burgers equation (4.1) in $[-1, 1]$, subject to the initial data

$$u(x, 0) = \frac{1}{4} + \frac{1}{2}\sin \pi(x + 0.2), \qquad -1 \le x \le 1, \tag{4.2}$$

and to the time-dependent inflow boundary condition

$$u(-1, t) = v(-0.8, t).$$

Here, v denotes the exact solution of (4.1) in a periodic domain $[-1, 1]$ subject to the initial data (4.2). This exact solution v is smooth until $T = 2/\pi$, then it develops a moving shock
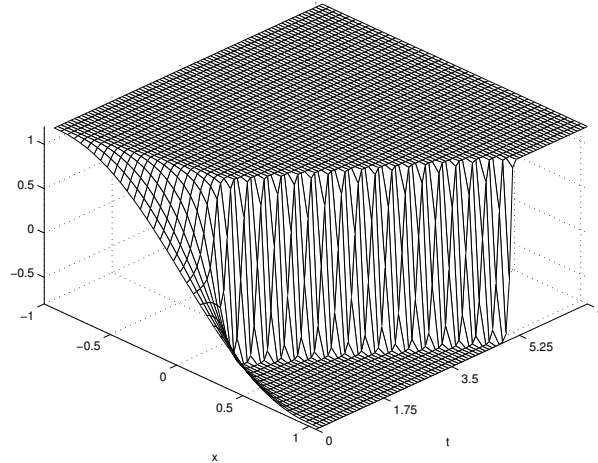
Figure 5: one dimensional Burgers equation (N=41)

which interacts with rarefaction waves. Note that there is a sonic point. The right boundary is an outflow boundary and hence we prescribe no additional boundary conditions there.

In Figure 6 we plot the approximate solution at time $T = 1.1$, i.e., after the development of discontinuity in the inflow boundary condition. We clearly see that our boundary treatment is accurate and stable even in the presence of a shock entering from the time-dependent inflow boundary.

2D Burgers equation

Here, we approximate the solution to the two-dimensional Burgers equation

$$u_t + \left(\frac{u^2}{2}\right)_x + \left(\frac{u^2}{2}\right)_y = 0, \tag{4.3}$$

subject to the initial conditions,

$$u_0(x, y) = \begin{cases} 0.5 & -1 \le x < 0, \quad -1 \le y < 0, \\ 0.0 & 0 \le x \le 1, \quad -1 \le y < 0, \\ -1.0 & 0 \le x \le 1, \quad 0 \le y \le 1, \\ -0.2 & -1 \le x < 0, \quad 0 \le y \le 1, \end{cases}$$

and augmented with boundary conditions at the inflow boundaries which are equal to the initial values at these same boundaries. The solution is approximated using the algorithm of §3.3. Figures 7-8 show contour plots of the solution at time $T = 2$ with mesh sizes 41×41, 81×81, 161×161 and 321×321. Again, we observe that there are no spurious oscillations at the boundaries, oscillations that are inherent with a naive treatment of inflow boundaries.
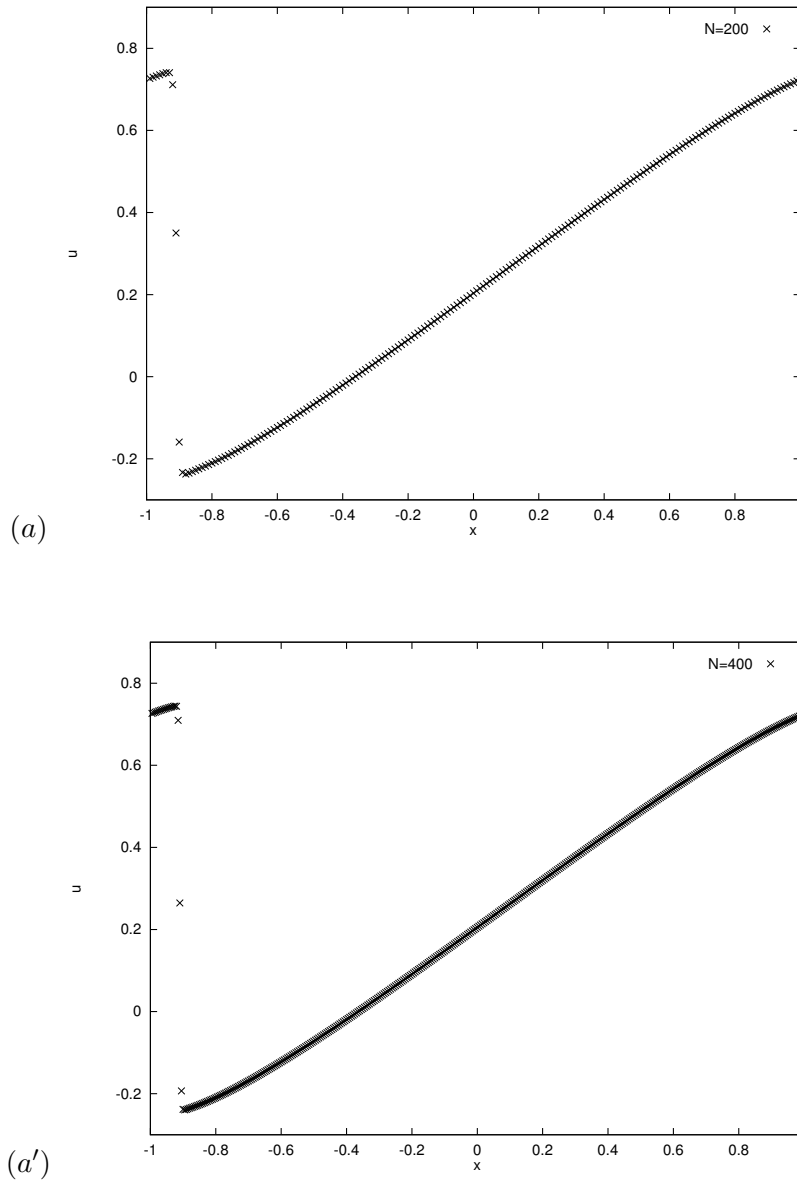
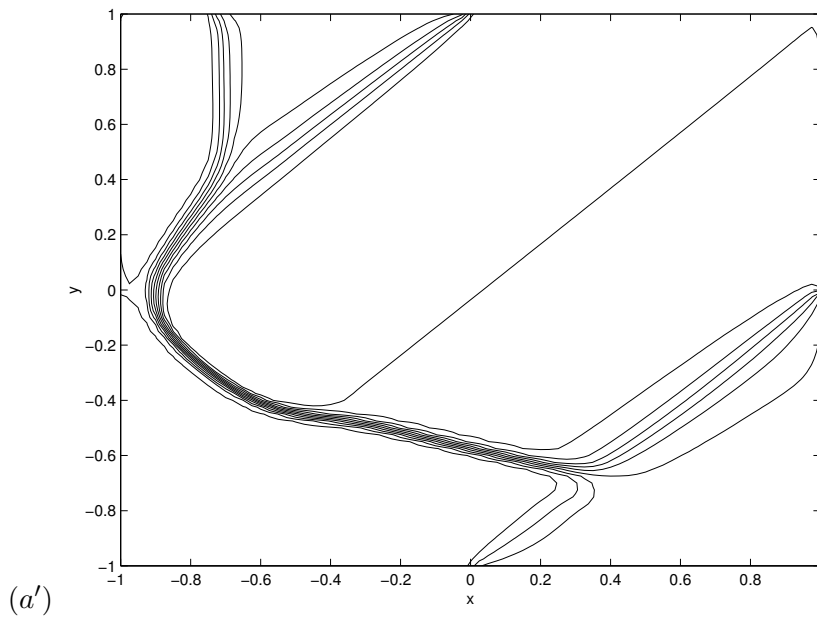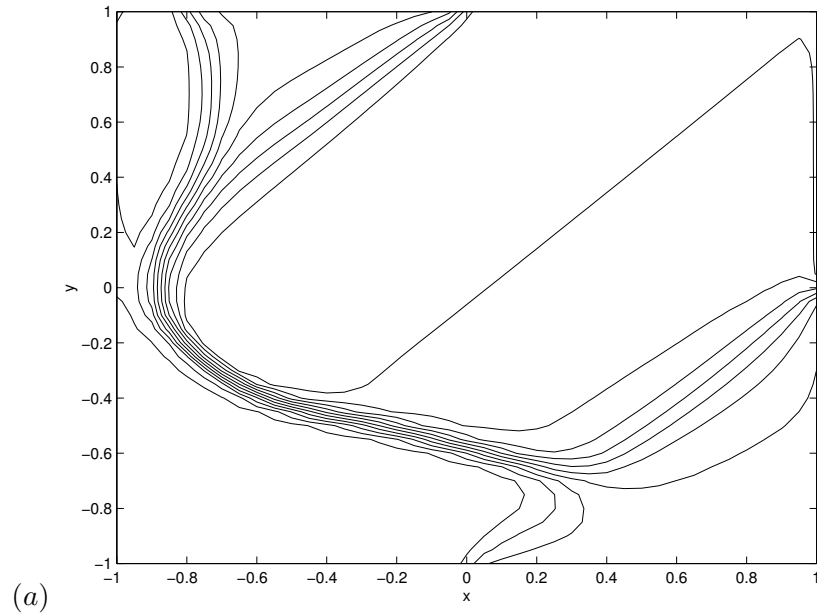Figure 6: Burgers equation. Shock entering from the time-dependent left boundary. T=1.1 (a) N=200, (a') N=400

Figure 7: The 2D IBVP Burgers equation: T=2. (a) N=41, (a') N=81
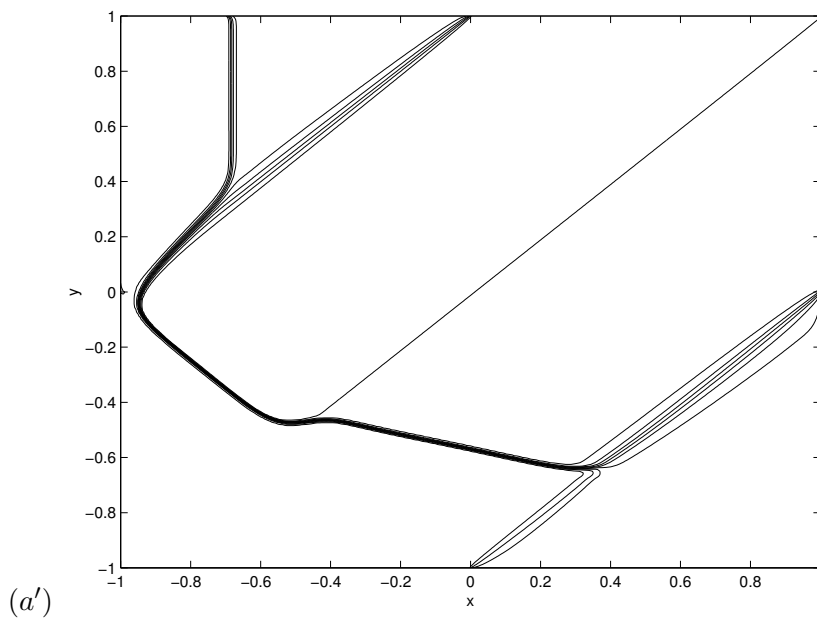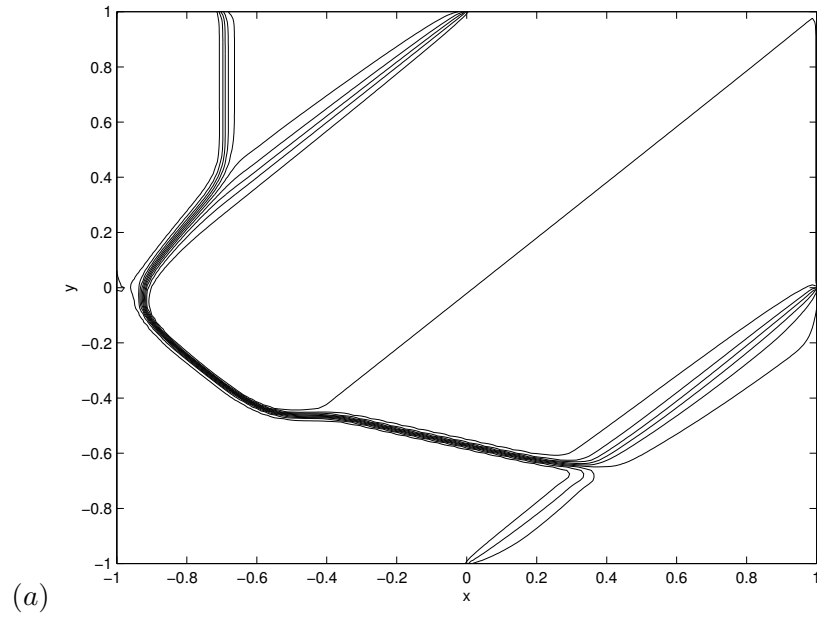
16   D. Levy and E. Tadmor

(a)

(a')

Figure 8: The 2D IBVP Burgers equation: T=2. (a) N=161, (a') N=321

References

[1] Arminjon P., Stanescu D., Viallon M.-C., *A Two-Dimensional Finite Volume Extension of the Lax-Friedrichs and Nessyahu-Tadmor Schemes for Compressible Flow*, Proc. 6th. Int. Symp. on CFD, Lake Tahoe, 1995, M. Hafez and K. Oshima, editors, Vol. IV, pp.7-14.

[2] Arminjon P., Viallon M.-C., *Généralisation du Schéma de Nessyahu-Tadmor pour Une Équation Hyperbolique à Deux Dimensions D'espace*, C.R. Acad. Sci. Paris, **t. 320** , série I. (1995), pp. 85-88.

[3] Bereux F., Sainsaulieu L., *A Higher Order Method for the Solution of Hyperbolic Systems with Relaxation*, preprint.

[4] Bianco F., Puppo G., Russo G., *High Order Central Schemes for Hyperbolic Systems of Conservation Laws*, SIAM J. Sci. Comp., to appear.

[5] Cockburn B., Shu C.-W., *TVD Runge-Kutta Local Projection Discontinuous Galerkin Finite Element Method for Conservation Laws II: General Framework*, Math. Comp., **52**, (1989), pp.411-435.

[6] Friedrichs K. O., Lax P. D., *Systems of Conservation Equations with a Convex Extension*, Proc. Nat. Acad. Sci., **68**, (1971), pp.1686-1688.

[7] Godlewski E., Raviart P.-A., *Numerical Approximation of Hyperbolic Systems of Conservation Laws*, Springer, New York, 1996.

[8] Harten A., *High Resolution Schemes for Hyperbolic Conservation Laws*, JCP, **49**, (1983), pp.357-393.

[9] Huynh H. T., *A Piecewise-parabolic Dual-mesh Method for the Euler Equations* (1995), preprint.

[10] Jiang G.-S., Tadmor E., *Nonoscillatory Central Schemes for Multidimensional Hyperbolic Conservation Laws*, SIAM J. Sci. Comp., to appear.

[11] Jin S., private communication.

[12] Katsaounis T., Levy D., *A Modified Structured Central Scheme for 2D Hyperbolic Conservation Laws*, Appl. Math. Let., to appear.

[13] van Leer B., *Towards the Ultimate Conservative Difference Scheme, V. A Second-Order Sequel to Godunov's Method*, JCP, **32**, (1979), pp.101-136.

[14] LeVeque R. J., *Numerical Methods for Conservation Laws*, Lectures in Mathematics, Birkhauser Verlag, Basel, 1992.

[15] Levy D., *A Third-order 2D Central Schemes for Conservation Laws*, INRIA School on Hyperbolic Systems, Vol. I (1998), pp.489-504.

[16] Levy D., Puppo G., Russo G. *Central WENO Schemes for Hyperbolic Systems of Conservation Laws*, M2AN, in press.

[17] Levy D., Puppo G., Russo G., *A Third Order Central WENO Scheme for 2D Conservation Laws*, submitted.

[18] Levy D., Tadmor E., *Non-oscillatory Central Schemes for the Incompressible 2-D Euler Equations*, Math. Res. Let., **4**, (1997), pp.321-340.

[19] Liu X.-D., Tadmor E., *Third Order Nonoscillatory Central Scheme for Hyperbolic Conservation Laws*, Numer. Math., **79**, (1998), pp.397-425.

[20] Nessyahu H., Tadmor E., *Non-oscillatory Central Differencing for Hyperbolic Conservation Laws*, JCP, **87**, no. 2 (1990), pp.408-463.

[21] Osher S., Tadmor E., *On the Convergence of Difference Approximations to Scalar Conservation Laws*, Math. Comp., **50**, no. 181 (1988), pp.19-51.

[22] Roe P. L., *Approximate Riemann Solvers, Parameter Vectors, and Difference Schemes*, JCP, **43**, (1981), pp.357-372.

[23] Runborg O., *Multiphase Computations in Geometrical Optics*, UCLA CAM report no. 96-52 (1996).

[24] Sanders R., *A Third-order Accurate Variation Nonexpansive Difference Scheme for Single Conservation Laws*, Math. Comp., **41** (1988), pp.535-558.

[25] Sanders R., Weiser A., *A High Resolution Staggered Mesh Approach for Nonlinear Hyperbolic Systems of Conservation Laws*, JCP, **1010** (1992), pp.314-329.

[26] Shu C.-W., *TVB Boundary Treatment for Numerical Solutions of Conservation Laws*, Math. Comp., **49**, no. 179 (1987), pp.123-134.

[27] Sweby P. K., *High Resolution Schemes Using Flux Limiters for Hyperbolic Conservation Laws*, SINUM, **21**, no. 5 (1984), pp.995-1011.

[28] Tadmor E., Wu C.C., *Central Scheme for the Multidimensional MHD Equations*, in preparation.